THE JOURNAL OF PHYSICAL CHEMISTRY B

Article

pubs.acs.org/JPCB

Mixing MARTINI: Electrostatic Coupling in Hybrid Atomistic–Coarse-Grained Biomolecular Simulations

Tsjerk A. Wassenaar,[†] Helgi I. Ingólfsson,[†] Marten Prieß,[‡] Siewert J. Marrink,[†] and Lars V. Schäfer*[,‡]

[†]Groningen Biomolecular Sciences and Biotechnology Institute & Zernike Institute for Advanced Materials, University of Groningen, Nijenborgh 7, 9747 AG Groningen, The Netherlands

[‡]Institute of Physical and Theoretical Chemistry, Goethe University Frankfurt, Max-von-Laue-Straße 7, D-60438 Frankfurt am Main, Germany

Supporting Information

ABSTRACT: Hybrid molecular dynamics simulations of atomistic (AA) solutes embedded in coarse-grained (CG) environment can substantially reduce the computational cost with respect to fully atomistic simulations. However, interfacing both levels of resolution is a major challenge that includes a balanced description of the relevant interactions. This is especially the case for polar solvents such as water, which screen the electrostatic interactions and thus require explicit electrostatic coupling between AA and CG subsystems. Here, we present and critically test computationally efficient hybrid AA/CG models. We combined the Gromos atomistic force field with the MARTINI coarse-grained force field. To enact electrostatic coupling, two recently developed CG water models with explicit electrostatic interactions were used: the polarizable MARTINI water model and the BMW model. The hybrid model was found to be sensitive to the strength of the AA–CG electrostatic coupling, which was adjusted through the relative dielectric permittivity ε_r(AA–CG). Potentials of mean force (PMFs) between pairs of amino acid side chain analogues in water and partitioning free enthalpies of uncharged amino acid side chain analogues between apolar solvent and water show significant differences between the hybrid simulations and the fully AA or CG simulations, in particular for charged and polar molecules. For apolar molecules, the results obtained with the hybrid AA/CG models are in better agreement with the fully atomistic results. The structures of atomistic ubiquitin solvated in CG water and of a single atomistic transmembrane α-helix and the transmembrane portion of an atomistic mechanosensitive channel in CG lipid bilayers were largely maintained during 50–100 ns of AA/CG simulations, partly due to an overstabilization of intramolecular interactions. This work highlights some key challenges on the way toward hybrid AA/CG models that are both computationally efficient and sufficiently accurate for biomolecular simulations.

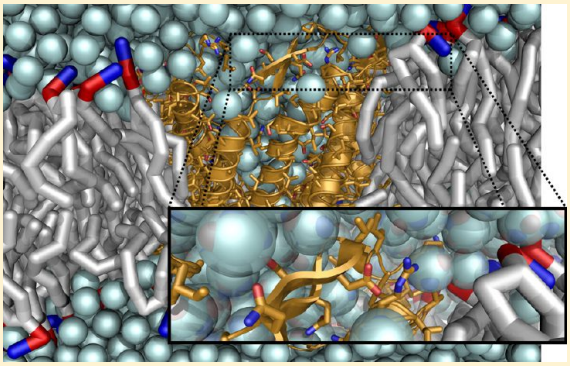

INTRODUCTION

Molecular dynamics (MD) simulations have been successfully used to study the structure and dynamics of biomolecular systems.[1−4] However, the large computational effort of conventional all-atom (AA) MD simulations severely limits the accessible length and time scales. Coarse-grained (CG) models that combine several atoms into CG beads have been developed that can increase computational efficiency by up to several orders of magnitude.[5−7] Such particle-based CG models have been applied to a broad range of biomolecular processes, such as lipid bilayer structure and dynamics,[8−12] protein folding,[13,14] and protein–lipid[15−17] as well as protein–protein interactions.[18−28] Despite this success, the reduced accuracy due to the inherent simplifications still limits the systems and processes that can be studied with CG models.

The aim of multiscale modeling is to overcome these limitations by combining different levels of resolution. Multiscale methods can be classified into sequential (or serial) and hybrid (or parallel) approaches.[29] Sequential methods use information obtained at a higher level of resolution, for example AA, to parametrize a lower-resolution model, for example CG.[12,29,30] Inverse mapping (or back-mapping) methods generate structures at a high level of resolution from their low-level counterparts.[31−39] By contrast, in hybrid methods, particles described at different levels of resolution are present simultaneously in the same simulation, thus requiring direct interactions between them. This can for example be implemented by spatially partitioning the simulation system into different regimes. In fixed-resolution AA/CG methods, a predefined set of atoms or molecules is described at the AA level, whereas a CG model is used for the remainder of the system, analogous to conventional quantum mechanics/molecular mechanics (QM/MM) methods.[40,41] Reducing computational cost is a main goal of multiscale modeling.

Received: November 22, 2012
Revised: January 25, 2013

Hence, a CG description of the solvent molecules is particularly appealing, since these usually represent the largest part of the system.

A key challenge in hybrid modeling is how to couple the different levels of resolution, i.e., how to describe the AA/CG interactions. Shi and co-workers[42] reparametrized the AA/CG interactions through force matching[12,43] to simulate an atomistic transmembrane peptide in a CG environment. A different approach was followed by Michel and co-workers.[44,45] Mixed AA/CG Lennard-Jones interactions were derived using standard mixing rules, and mixed charge−charge and charge−dipole interactions were calculated using the standard formulas employed in the pure models. Additional scaling parameters were found to be necessary for both Lennard-Jones and electrostatic AA/CG interactions, with the optimal scaling parameter depending on the system. Masella and co-workers[46,47] combined a polarizable pseudoparticle solvent with a polarizable atomistic force field. In this model, the solvent dipoles only interact with the solute, not with themselves. In all the above studies, models that map one water molecule to one CG bead were used, thus limiting the computational speedup with respect to a fully atomistic treatment. Rzepiela and co-workers[48] devised a hybrid model in which the MARTINI force field[49] was used for the CG part. Since a single CG water bead represents four water molecules in the MARTINI model, a significant gain in computational efficiency could be achieved. For the mixed AA/CG interactions, virtual CG interaction sites were introduced on groups of solute atoms. The forces on these virtual CG sites due to the surrounding, described at the level of the CG force field, were redistributed over the atomistic particles. A drawback of this approach is that the standard MARTINI water model is a pure Lennard-Jones fluid and thus cannot mediate any explicit dielectric screening. Due to this limitation, Rzepiela and co-workers[48] introduced a relative dielectric permittivity, ε_r, to uniformly screen the AA−AA Coulomb interactions. It was found that the value of ε_r required for dialanine in apolar solvent differs from that in water, implying that this approach cannot be used for simulations of large heterogeneous systems, such as proteins, in which the electrostatic interactions between protein atoms are screened not only by the solvent but also by other protein atoms. Electrostatic coupling was also not included in the original model of Han and co-workers,[50−52] who combined a united-atom model that does not include any partial charges with the MARTINI model. The mixed Lennard-Jones interactions were reparametrized such that experimental solvation free energies of small organic compounds were reproduced. In a recent extension,[53] partial charges were introduced for charged amino acid side chains. However, AA and CG subsystems still did not interact through Coulomb potentials, since the standard Lennard-Jones MARTINI water model was used. All electrostatic interactions were screened by a uniform dielectric permittivity of $\varepsilon_r = 15$, the value used in the MARTINI force field. Notably, this approach enabled folding simulations of several small proteins.[53] Very recently, Riniker and co-workers[54] presented a model with explicit electrostatic coupling of AA and CG subsystems. A polarizable two-site CG dipole water model representing five atomistic water molecules was used.[55] Using mixtures of atomistic and CG water molecules, the dielectric permittivity for the AA/CG Coulomb interactions, ε_r(AA−CG), was adjusted, while AA/CG Lennard-Jones interactions were derived from standard combination rules.[54] From structural analysis of 20-ns MD simulations of four small proteins in CG water, it was concluded that there are no large differences compared to fully atomistic simulations, apart from an increased tendency to form protein−protein hydrogen bonds.[56] In the above models, entire molecules were assigned to either the AA subsytem or the CG subsystem. In the AA/CG approach of Neri and co-workers,[57] the active site of a protein was described atomistically and the remainder was described with a CG model. An interface region was introduced to embed the AA subsystem into the CG protein. Mixed AA/CG electrostatic interactions were not accounted for, since a simple Go-type CG model was used and explicit bulk solvent was neglected.

In contrast to the above fixed partitioning methods, in which the assignment of the particles to the AA and CG regimes cannot change during the simulation, adaptive resolution methods allow molecules to change resolution on the fly, depending on their spatial coordinates.[58−61] Applications of adaptive AA/CG methods thus far mainly focused on rather simple test systems,[62] with recent extensions toward solvated polymers[63,64] and adaptive QM/MM.[64−66] An alternative to the spatial partitioning schemes are Hamiltonian exchange methods, in which different representations of a system evolve concurrently and can swap resolution. At least partly owing to their conceptual complexity, such methods have hitherto only been applied to alkanes and small peptides.[67−69]

In this work, we investigate the effect of including an explicit electrostatic coupling of AA and CG subsystems in hybrid AA/CG simulations employing the MARTINI model[49] for the CG part. MARTINI was parametrized for various biomolecules, such as lipids,[49] proteins,[70] and carbohydrates,[71] thus enabling a broad range of possible applications. Recently, two CG water models that can be used in conjunction with the MARTINI force field were developed that include (partial) charges and thus explicitly screen the Coulomb interactions: the polarizable MARTINI water (PW) model[72] and the big multipole water (BMW) model.[73,74] Like standard MARTINI water, both models use a 4-to-1 mapping of AA to CG water molecules and thus provide a substantial computational speedup compared to simulations with atomistic solvent. In the hybrid model presented here, we combined the PW and BMW models with different parameter sets of the Gromos force field[75−77] for the solutes. AA and CG subsystems directly interact via Coulomb potentials, which were adjusted through the relative dielectric permittivity, ε_r(AA−CG). To assess the quality of the hybrid model, potentials of mean force (PMFs) between small solutes in water, such as the Na^+/Cl^- ion pair and amino acid side chain analogues, were compared to the fully atomistic (using the SPC/E water model[78]) and fully CG simulations. In addition, we tested a hybrid model recently proposed by Riniker and co-workers.[54,56] We also investigated the different models in terms of partitioning free enthalpies of uncharged amino acid side chain analogues between water and apolar solvent. Furthermore, hybrid simulations of atomistic proteins (or polypeptides) embedded in a CG environment were compared to fully atomistic simulations. The systems chosen for this purpose are the GCN4-p1 peptide and ubiquitin in water, the WALP23 transmembrane α-helix embedded in a dipalmitoylphosphatidylcholine (DPPC) lipid bilayer, and the transmembrane part of the mechanosensitive channel of large conductance (MscL) embedded in a dioleoylphosphatidylcholine (DOPC) bilayer.

The rest of the article is organized as follows: First, we describe the hybrid model and simulation setup. We then

dx.doi.org/10.1021/jp311533p | J. Phys. Chem. B XXXX, XXX, XXX−XXX

present and discuss the PMFs and partitioning free enthalpies. We proceed with the results of hybrid AA/CG simulations of selected proteins/polypeptides in water and lipid bilayer environment. A general discussion and a short conclusive section end this article.

METHODS

Hybrid Model. We will first briefly describe the concept of the previous scheme of Rzepiela and co-workers[48] and then line out the extension to our new model. The general idea of hybrid AA/CG models is to describe a part of the system atomistically, while modeling the rest with an efficient CG force field. In the previous model of Rzepiela and co-workers,[48] the interactions between particles belonging to the same resolutions (i.e., AA−AA and CG−CG) were described by the respective "pure" force fields without further alterations. The coupling between the different levels of resolution, i.e., the AA−CG interactions, was described at the CG level. This was achieved through virtual CG interaction sites placed at the center of mass of the corresponding atomistic particles (according to the AA/CG mapping). The forces acting on the virtual sites due to the CG potentials were distributed over the corresponding atomistic particles such that the total force and torque are conserved. Interactions between virtual sites, interactions between virtual sites and atomistic particles, and direct interactions between atomistic and CG particles were excluded. This approach is simple and modular: Ideally, it does not require the parametrization of any AA−CG cross-interactions and in principle it enables the combination of any AA and CG force fields.

The new hybrid AA/CG scheme presented here includes explicit dielectric screening of the AA−AA interactions due to the charged CG particles, which requires direct Coulomb interactions between AA and CG particles. This was put into action by using reaction field potentials and forces,[79] $V_{rf} = q_i q_j/(4\pi\varepsilon_0\varepsilon_r)(r_{ij}^{-1} + k_{rf} r_{ij}^{2} - c_{rf})$ and $F_{rf} = q_i q_j/(4\pi\varepsilon_0\varepsilon_r)(r_{ij}^{-2} - 2k_{rf} r_{ij})$, respectively, with $k_{rf} = r_c^{-3}(\varepsilon_{rf} - \varepsilon_r)(2\varepsilon_{rf} + \varepsilon_r)^{-1}$ and $c_{rf} = r_c^{-1} + k_{rf} r_c^{2}$. Here, q_i and q_j are the charges on particles i and j, respectively, r_{ij} is the distance between the charges, ε_0 is the vacuum dielectric permittivity, ε_r is the relative dielectric constant, $\varepsilon_{rf} = 78$ is the dielectric constant of the continuum, and $r_c = 1.4$ nm is the cutoff. To apply different ε_r's for the different interactions (AA−AA, CG−CG, and AA−CG), the above potential and force were tabulated, with a spacing of 0.002 nm. The values used for the relative dielectric constant were $\varepsilon_r = 1$ for the AA−AA interactions and $\varepsilon_r = 2.5$, 1.3, and 15.0 for the CG−CG interactions in PW, BMW, and standard MARTINI water, respectively. We systematically varied ε_r for the AA−CG interactions to adapt the strength of the electrostatic coupling; see below. Charges on virtual CG sites (but not on regular CG particles) were put to zero; virtual CG sites were thus only used for the AA−CG Lennard-Jones interactions.

The PW[72] and BMW[73] CG water models were applied, which were parametrized to be used together with the MARTINI force field. Other CG water models for including dielectric solvation effects have been developed,[55,80,81] but not in conjunction with MARTINI; these were therefore not considered here, apart from the model of Riniker and van Gunsteren,[55] see below. Figure 1 illustrates the basic AA/CG scheme for the example of a small AA molecule surrounded by CG water. The PW model[72] comprises an uncharged central Lennard-Jones bead and two satellites with opposite charges

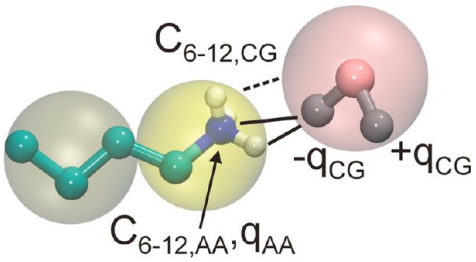

Figure 1. Concept of hybrid AA/CG simulations. Lennard-Jones interactions between AA and CG subsystems (dashed line) are treated at the level of the CG force field by using virtual CG interaction sites (transparent beads). Charged particles in the AA and CG systems interact via Coulomb potentials (solid lines). The interactions within the AA and CG subsystems are described by the respective force fields.

($\pm 0.46e$) that form the dipole. An angle potential between the three beads makes PW polarizable (orientational polarizability). By contrast, in the BMW model, all three particles are charged ($-2e$ on the central bead, $+1e$ on the satellites) and thus form a multipole. All internal degrees of freedom of the BMW water are constrained; i.e., it is a rigid model. The satellite beads in PW and BMW do not interact with other particles via Lennard-Jones potentials; i.e., there is no short-range Pauli repulsion. This is no problem in the CG simulations, because the charged sites are well within the excluded volume of the central particle (Figure 1). However, in the AA/CG simulations, overlapping charged AA and CG particles led to numerical instabilities. To avoid this polarization catastrophe, a short-ranged repulsion was introduced between the charged CG water satellites and atomistic particles, with a Lennard-Jones C_{12} parameter of 10^{-7} kJ mol^{-1} nm^{12}. To test this choice, the PMF between lysine and glutamate side chain analogues was recalculated using an extremely short-ranged repulsion of $C_{12} = 10^{-12}$ kJ mol^{-1} nm^{12}, which yielded the same PMF within the statistical error.

Simulation Setup. All simulations were performed with the Gromacs MD simulation package (version 4.5).[82] In the atomistic simulations, and for the atomistic subsystems in the hybrid simulations, the Gromos parameter sets 53a6[77] (Na^+/Cl^-, amino acid side chain and backbone analogues), 43a2[75] (GCN and WALP23), and 45a3[76] (ubiquitin and MscL) were used. The MARTINI force field (version 2.1)[49,70,72] was used for the CG (sub)systems. In the simulations with atomistic solvent, the SPC/E water model[78] was used. The temperature was kept constant at 298 K by using leapfrog stochastic dynamics[83] (SD integrator in Gromacs) with an inverse friction constant of $\tau_T = 2$ ps. The pressure was kept constant at 1 bar with a Berendsen barostat[84] (time constant $\tau_p = 1$ ps). The integration time step was 2 fs (20 fs in the fully CG simulations), constraining bond lengths with LINCS[85,86] (and SETTLE,[87] for SPC/E). Nonbonded interactions within 1.4 nm were calculated at every time step, and the charge group based neighbor list was updated every 10 steps within this cutoff (every five steps in the fully CG simulations). As described above, a reaction field contribution was added to the electrostatic interactions beyond the long-range cutoff. For the van der Waals interactions, Lennard-Jones (LJ) 6,12 potentials were used. For the AA−AA LJ interactions, a plain cutoff of 1.4 nm was applied, whereas the CG−CG and virtual site−CG LJ potentials were smoothly shifted to zero between 0.9 and 1.2 nm. The BMW−BMW van der Waals interactions were described with a soft Born−Mayer−Huggins potential.[73]

dx.doi.org/10.1021/jp311533p | J. Phys. Chem. B XXXX, XXX, XXX−XXX

Potential of mean force (PMF) calculations were carried out in both AA and CG water. Two solute molecules were solvated with 2400 SPC/E or 600 CG water molecules (one CG water molecule represents four atomistic waters) in a periodic rhombic dodecahedron unit cell of 4.6 nm. The PMFs were calculated between the following molecule pairs: charged (Na^+/Cl^-, Lys^+/Glu^-, Arg^+/Glu^-, Glu^-/Glu^-), polar (Ser/Ser, NMA/NMA, where NMA is *n*-methylacetamide), and apolar (Phe/Phe, Val/Val). The amino acids were represented by their respective side chain analogues, and NMA was included as a backbone analogue. The PMF was calculated from a set of distance constraint simulations according to[88] $V_{mf} = \int_{R_m}^{r} dr\,[\langle f_c \rangle_r + 2k_B T r^{-1}]$, where $\langle f_c \rangle_r$ is the ensemble average of the constraint force between the centers of mass of the two molecules that are separated by a constraint of length r, and R_m is the maximum distance up to which the PMFs were calculated. A relative free energy of zero was assigned to the configuration at R_m. The LINCS algorithm[85,86] was used to constrain the distance between the two molecules. The basic distance spacing was 0.05 nm; additional points were introduced where necessary. Thus, ca. 40 constraint simulations were necessary to cover the typically sampled distance range from 0.25 nm up to R_m = 2.2 nm. To generate starting structures, solvated configurations at each 0.05 nm were generated and energy minimized (steepest descent, 1000 steps). The sampling time was 10 ns at each constrained distance, the first 100 ps of which were discarded in the analysis of $\langle f_c \rangle_r$. Statistical errors were estimated from the limiting values of the block averages, as described by Hess[89] and implemented in the g_analyze tool of Gromacs. Two additional tests were done to check and validate our PMF calculations. First, to investigate the influence of the limited sampling time, the PMF between two AA serine side chains in PW was calculated using a sampling time of 100 ns at each distance, which, within the statistical error, yielded the same PMF as with 10-ns sampling. Second, an extended 5000-ns MD simulation of two mobile (i.e., unconstrained) CG phenylalanine side chains solvated in PW was carried out, and the PMF was calculated from the pair correlation function $g(r)$ according to $V_{mf} = -k_B T \ln g(r)$. The obtained PMF was virtually identical to the one from the distance constraint simulations. We used the constraint method because it provides equal sampling of all relevant configurations, including the energy barriers, and is thus computationally more efficient than the brute force approach.[90,91] The validity of the PMFs at the fully atomistic and fully CG level reported here is further supported by the agreement with recently published data.[92]

Thermodynamic integration (TI) calculations were carried out to determine the free enthalpies of solvation in CG water and in CG butane. In these calculations, single amino acid side chain analogues were solvated with 160 CG water or butane molecules in a periodic rhombic dodecahedron unit cell. We restricted our study to the amino acid side chains that are uncharged at pH 7; in addition, Ala, Gly, His, and Pro were not considered. In the TI calculations, all nonbonded interactions between solute and solvent were turned off using a coupling parameter λ. Soft-core potentials were used for the nonbonded interactions,[93] $V_{sc} = (1 - \lambda)V(\alpha\sigma^6\lambda^p + r^6)^{1/6}$, with potential height α = 0.6, interaction range σ = 0.3 nm, and λ power p = 1.[94,95] A spacing between the λ-points of 0.05 was used; thus 21 λ-points span the entire range between λ = 0 (fully coupled state) and λ = 1 (fully uncoupled state). To generate initial configurations, the solutes were solvated at the correct density and energy minimized at the respective λ-point (1000 steps steepest descent). The sampling time was 500 ps at each λ-point, the first 100 ps of which was discarded in the analysis of $dG/d\lambda$. Statistical uncertainties were estimated using block averaging, analogous to the PMF calculations described above; in general, statistical errors were below 2 kJ/mol. In the hybrid AA/CG TI calculations, reaction field electrostatics was used, as done in all PMF calculations and described above. A different approach was adopted in the TI calculations at the fully CG level: For the CG solutes in PW, the MARTINI shifted cutoff scheme was used. For the CG solutes in BMW, particle-mesh Ewald[96] with a grid spacing of 0.2 nm was used, as suggested by Wu and co-workers.[73,74] This procedure was followed to be able to quantitatively compare our free enthalpies to the literature.[72,74] The $dG/d\lambda$ curves were integrated using the trapezoidal rule. As an independent test, Bennett's acceptance ratio method[97] was applied, as implemented in the g_bar tool of Gromacs. The results obtained with both methods were the same within the statistical errors. Furthermore, to test a possible influence of the number of solvent molecules, the TI calculations of the atomistic Ser and Trp side chain analogues were repeated in large boxes containing 600 (instead of 160) PW molecules, again yielding the same results.

For the simulations of the GCN4-p1 peptide, the first structure from the NMR bundle in PDB 2OVN[98] was taken and solvated with 1826 SPC water molecules or 1000 PW water beads, respectively, in a periodic cubic simulation box. Counterions were not added, because the simulated GCN peptide had no net charge, thus circumventing any possible artifacts due to counterions (see below). After energy minimization (1000 steps steepest descent), the water was equilibrated with positional restraints on the protein heavy atoms (force constant 1000 kJ mol^{-1} nm^{-2}). Finally, 100-ns free MD simulations were carried out in the NPT ensemble by coupling to a pressure bath at 1 bar (τ_p = 0.5 ps) and temperature bath at 300 K using the velocity rescaling thermostat of Bussi and co-workers[99] with a time constant of τ_T = 0.1 ps.

For the ubiquitin simulations, the protein structure was taken from PDB 1UBI[100] and solvated with 9260 SPC molecules or 2315 PW water beads in a periodic rhombic dodecahedron box. Also in this case, the simulation box was uncharged and thus no counterions were added. The rest of the simulation setup and parameters were identical to GCN described above.

To set up the simulations of the WALP transmembrane (TM) peptide, a single atomistic WALP23 peptide was embedded in a CG bilayer comprised of 368 DPPC molecules, solvated by 3379 CG water beads. The PW, BMW, and standard MARTINI water models were used; thus three AA/CG simulations were carried out in this case. In the simulations with the standard (Lennard-Jones only) MARTINI water model, the original scheme of Rzepiela et al.[48] was applied; i.e., there were no direct Coulomb interactions between the CG (zwitterionic PC headgroups) and AA subsystems. The lateral and normal box vectors were separately coupled to a pressure bath at 1 bar (semi-isotropic coupling scheme, τ_p = 0.5 ps), and peptide, DPPC, and water molecules were coupled separately to a velocity rescaling thermostat[99] at 323 K (τ_T = 0.1 ps). The other simulation parameters were the same as in the simulations described above. The initial configuration for these AA/CG simulations was taken from our previous study, in which we back-mapped a CG WALP23 peptide embedded in

dx.doi.org/10.1021/jp311533p | J. Phys. Chem. B XXXX, XXX, XXX−XXX

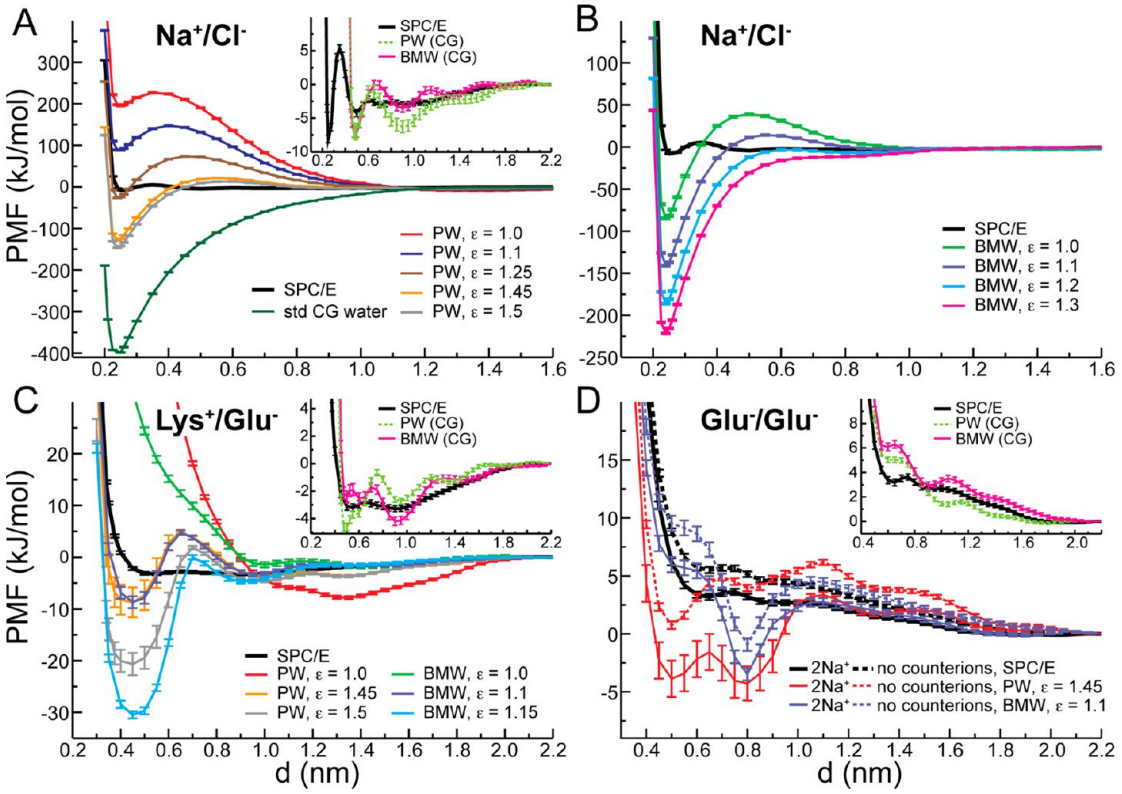

Figure 2. Potentials of mean force between univalent ions in water. (A and B) Atomistic Na^+/Cl^- ion pair in coarse-grained water. (A, inset) Fully AA and CG simulations. (C and D) Atomistic Lys^+/Glu^- and Glu^-/Glu^- pairs in CG water, respectively. (C and D, inset) Fully AA and CG simulations for Lys^+/Glu^- and Glu^-/Glu^-, respectively.

a CG bilayer comprised of 368 DPPC and 224 cholesterol molecules to the underlying atomistic representation.[23] Water and cholesterol molecules were removed from this system, and the DPPC lipids (but not the WALP23 peptide) were reconverted to the MARTINI-CG representation. The resulting system was rehydrated with CG water, taking care that no water was introduced in the hydrophobic interior of the bilayer. The resulting hybrid AA/CG system was subsequently energy minimized (1000 steps steepest descent) and simulated for 10 ns with harmonic position restraints (force constant 1000 kJ mol^{-1} nm^{-2}) on the WALP23 atoms, during which the box dimensions were allowed to relax (semi-isotropic pressure coupling). Finally, 60-ns simulations were carried out at the AA/CG level.

The mechanosensitive channel of large conductance (MscL) senses tension in the cell membrane. MscL has been extensively studied using both atomistic and coarse-grained MD simulations.[101−107] Simulating an atomistic MscL in a CG environment would enable resolution of the atomistic details of MscL gating without the computational overhead of an AA environment. For our hybrid MscL simulations an atomistic MscL was immersed in a CG lipid bilayer composed of 369 DOPC lipid molecules and solvated by 7109 CG water beads. Additionally, for the simulations that included ions, ∼100 mM NaCl was added by replacing randomly selected water beads with 51 Na^+ and 66 Cl^- CG-MARTINI ions. The MscL structure used was the closed state crystal structure from *Mycobacterium tuberculosis* (PDB 2OAR)[108] with the water exposed C-terminal helix (Glu104 to Asn125) removed. C-terminus deleted MscL channels have been shown to be functional in vitro.[109] The simulation parameters were the same as for the WALP peptide, except the bath temperature was set to 303 K with a time constant of τ_T = 1.0 ps and τ_p = 3 ps for the pressure coupling. The MscL structure was energy-minimized in vacuo (500 steps steepest descent), and CG DOPC lipid molecules were placed on a grid surrounding the MscL, spaced 0.65 nm apart (in the plane of the bilayer). CG water beads (and ions) were also placed on a grid, filling the simulation box, excluding space already filled with the protein, lipids, and a 3 nm slap defining the bilayer hydrophobic core. The resulting system was energy minimized (500 steps steepest descent). Then, the CG particles were relaxed with harmonic position restraints on the MscL heavy atoms (force constant 1000 kJ mol^{-1} nm^{-2}), starting with 20 ps NVT MD simulation using a 1-fs time step, followed by another 20 ps with pressure coupling, and then 2 ns with a 2-fs time step. Finally, free (i.e., unrestrained) MD simulations for each MscL system were carried out for 100 ns in the NPT ensemble.

To generate multiscaled structures and topologies for proteins, here in particular for MscL, several options were added to the recently introduced program, martinize.py,[110] for building MARTINI coarse-grained structures and topologies. When used for multiscaling, the program will generate the virtual CG sites that correspond to the atomistic structure, together with the AA/CG mapping. These can be added to the structure and topology, respectively, to generate the multiscale model. For further facilitation, an additional shell script was written, containing a complete protocol for automated coarse-grained and multiscale simulations, taking care of the bookkeeping involved in merging the atomistic structure with the virtual sites. This program, called martinate.sh, is the equivalent of the atomistic simulation protocol powering the

dx.doi.org/10.1021/jp311533p | J. Phys. Chem. B XXXX, XXX, XXX−XXX

recently presented Gromacs GRID portal[111] and was used to set up the MscL simulations. Both martinize.py and martinate.sh are made available via the Web sites www.cgmartini.nl and www.molecular-dynamics.net.

RESULTS AND DISCUSSION

Potentials of Mean Force (PMFs) in Water. We first present the results for pairs of univalent ions (Na^+/Cl^- as well as Lys^+/Glu^- and Glu^-/Glu^-) and then, for uncharged molecules, both polar (Ser/Ser side chain analogues and NMA/NMA, where *n*-methylacetamide (NMA) represents an amino acid backbone analogue), and apolar (Phe/Phe and Val/Val side chain analogues).

Na^+/Cl^-. The results for the Na^+/Cl^- ion pair are shown in Figure 2A,B. Although Na^+/Cl^- may be considered a rather simple case, it is a challenge for our AA/CG model, because the high charge density due to the localization of a full point charge on a single atom can be expected to strongly polarize the surrounding CG water molecules.

The PMFs from the fully AA and CG simulations are shown in Figure 2A (inset). In SPC/E (black curve), the contact minimum at a distance of 0.25 nm is separated by an energy barrier (desolvation peak) at 0.35 nm from the solvent-separated minimum at 0.5 nm. The relative free energies are −8.0, +5.0, and −4.0 kJ/mol, respectively (see Supporting Information Table S1 for relevant maxima and minima of all PMFs). These energies are reasonable, taking into account that different combinations of atomistic ion and water force fields yield slightly different PMFs.[88,112,113] The PMFs from the fully CG simulations (green, PW; magenta, BMW) are similar to the atomistic PMF in that a contact minimum is separated from a solvent-separated minimum by a barrier. The main difference between AA and CG ions is their size: A CG Na^+ or Cl^- ion effectively represents an AA ion with its first solvation shell. Consequently, in the CG PMFs, the location of the first minimum at 0.5 nm corresponds to the second (solvent-separated) minimum in the AA PMF. Furthermore, in CG water, the PMFs display a number of secondary peaks up to long distances. This overstructuring is due to the size of the CG water (one CG water bead represents four atomistic water molecules), and is slightly worse in PW than in BMW, because the former uses a LJ potential with a steep r^{-12} term for the Pauli repulsion, as compared to the softer Born−Mayer−Huggins potential used for the latter.[73] The higher barriers are due to the solvent granularity, which may be reminiscent of depletion forces known from colloid and polymer systems, and are also observed in the hybrid AA/CG simulations (see below).

We now turn to the hybrid AA/CG model. We found that the PMFs are very sensitive to the coupling between AA and CG subsystems, determined by the relative dielectric constant ε_r(AA−CG). In PW, full coupling between AA and CG subsystems ($\varepsilon_r = 1$) leads to a repulsive PMF at intermediate distances and a high-energy minimum at 0.25 nm (Figure 2A, red curve). Weakening the electrostatic interactions between solutes and solvent gradually lowers the energy of both the minimum and the barrier. With ε_r(AA−CG) = 1.25 (brown curve), the location and energy of the contact minimum roughly corresponds to that in SPC/E; however, a high and broad barrier separates it from the dissociated state. The barrier height is further lowered with increasing ε_r. At ε_r(AA−CG) = 1.5 (gray), the free energies of the barrier and minimum are 13 and −145 kJ/mol, respectively. As a simple LJ fluid, standard MARTINI water cannot screen the Coulomb interactions, leading to a vacuumlike behavior with a very strong attraction of about −400 kJ/mol (green). Of course, this could be remedied by applying a (uniform) ε_r(AA−AA) > 1. However, as also shown below, such a primitive electrolyte model is not of general use[113] and was thus not further explored here. The PMFs in BMW (Figure 2B) are qualitatively similar to those in PW. The well depths and barrier heights strongly depend on ε_r(AA−CG), with weaker coupling corresponding to lower minima and barrier energies (the barrier vanishes for $\varepsilon_r \geq 1.2$). A minimum with an energy corresponding to the PMF in SPC/E can be obtained with ε_r(AA−CG) < 1; however, this leads to a very high energy barrier (data not shown).

Taken together, for Na^+/Cl^-, the PMFs from the hybrid AA/CG simulations are very different from the PMFs obtained from the fully AA and CG simulations. In general, the PMF between two solute molecules not only reflects the direct interaction between them, but is also affected by multibody contributions due to solute−solvent and solvent−solvent interactions, i.e., the solvent response to a particular solute configuration. In our AA/CG simulations, at small ε_r(AA−CG), the atomistic ions overpolarize the surrounding CG water molecules, leading to the observed high and broad barriers. This cannot be remedied by increasing ε_r, because that yields too deep minima. Thus, it appears that it is not possible to match the AA/CG PMFs with the reference PMFs through ε_r(AA−CG) as the only adjustable parameter. It should be noted that, in terms of their LJ radii with respect to the solvent (but not with respect to each other), the ions represent CG ions; i.e., the surrounding solvent molecules cannot closely approach the ions. It would thus appear reasonable in this case to implicitly account for the dielectric screening within the excluded volume through using ε_r(AA−AA) > 1. However, we did not further explore this possibility here, because the aim of studying the Na^+/Cl^- ion pair was not primarily to obtain a quantitative agreement with the AA simulations, but rather to explore the general behavior of the hybrid AA/CG model, as a basis for the subsequent study of molecular ions (for which such excluded volume effects should play a minor role).

To test our hypothesis that dielectric overpolarization, and not the cavity around the small ions, is the main contribution to the observed features in the PMFs, we calculated the PMF of atomistic NaCl in PW with the charges on the Na and Cl atoms set to zero. The resulting PMF (Figure 3B, orange curve) has a relatively shallow contact minimum at 0.3 nm (−6.0 kJ/mol) and a broad maximum at 0.65 nm (+3.1 kJ/mol), confirming that the large absolute energies of the minima and maxima observed in Figure 2A are indeed due to the electrostatic response of the CG water molecules. Interestingly, the energy of the contact minimum of the neutralized ions is of similar magnitude as the respective minimum for charged NaCl in SPC/E (Figure 3B, black). Whereas the latter is due to electrostatic attraction, the former arises from the (weak) dispersion attraction and possibly depletion forces due to the missing pressure compensation at solute−solute distances smaller than the size of a single CG solvent molecule.

Lys^+/Glu^-. Figure 2C shows the PMFs between the charged side chain analogues of Lys (*n*-butylammonium cation) and Glu (propionate anion). The polarization of the solvent is expected to be weaker than for Na^+/Cl^-, since the total charge is distributed over several atoms in these molecular ions and the magnitude of the partial charge on any individual atom is smaller than 1. Nevertheless, for ε_r(AA−CG) = 1, the AA/CG

dx.doi.org/10.1021/jp311533p | J. Phys. Chem. B XXXX, XXX, XXX−XXX

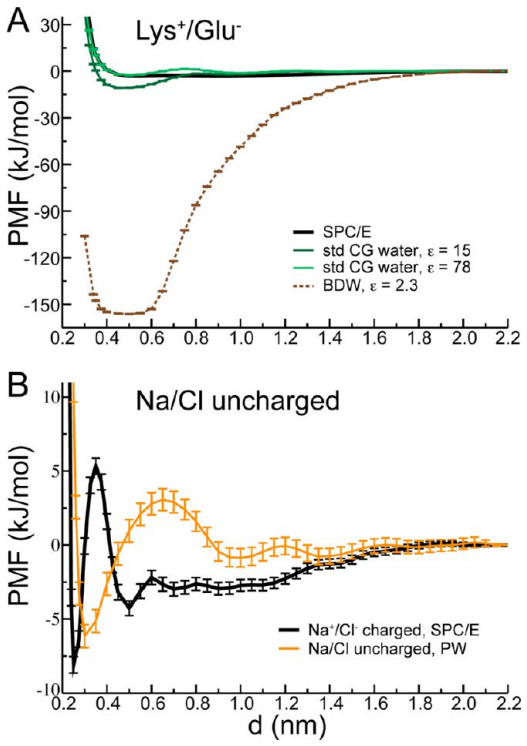

Figure 3. (A) PMF of atomistic Lys^+/Glu^- in CG water. BDW model (dashed brown curve); standard MARTINI water with ε_r = 15 and 78 (light and dark green curves, respectively) and in SPC/E water (black curve). (B) PMF of uncharged atomistic NaCl ion pair in CG water (orange). The PMF of (charged) Na^+Cl^- in SPC/E is shown in black.

PMFs in both PW (red curve) and BMW (green) are repulsive. For intermediate coupling strengths of ε_r(AA−CG) = 1.45 and 1.1 in PW (orange) and BMW (violet), respectively, the PMFs in PW and BMW are very similar to each other, with a contact minimum at 0.45 nm (−8.5 kJ/mol), a desolvation barrier at 0.65 nm (+5.0 kJ/mol), and a shallow solvent-separated minimum at 0.95 nm (−3.5 kJ/mol). The fully AA and CG reference PMFs (Figure 2C, inset) have less deep minima and smaller energy barriers. Although not explicitly tested, qualitatively similar results are expected for other charged side chains, such as Arg^+ and Asp^-.

In addition to using the PW and BMW CG water models in the hybrid scheme, we also calculated the PMF of the Lys^+/Glu^- pair using the AA/CG model suggested by Riniker and co-workers,[54,56] which involves using a CG dipole water model representing five water molecules[55] with ε_r(CG−CG) = 2.5 and ε_r(AA−CG) = 2.3 (this water model is referred to as the big dipole water (BDW) model). AA−CG Lennard-Jones interactions were described using the standard mixing rules. As shown in Figure 3A (dashed brown curve), this model yielded an unphysically deep minimum at −155 kJ/mol due to the rather weak electrostatic coupling between AA and CG subsystems. Figure 3A also shows the PMFs obtained with the standard Lennard-Jones MARTINI water model in combination with uniform dielectric permittivities of ε_r = 15 (i.e., the value used in the MARTINI CG force field) and 78, respectively. Although the PMF with ε_r = 78 matches the fully atomistic one reasonably well, this approach cannot be applied to large molecules with anisotropic charge distributions such as proteins,[114] as also shown below.

Glu^-/Glu^-. The PMF between two Glu^- anions is shown in Figure 2D. For the hybrid AA/CG simulations in PW and BMW, ε_r(AA−CG) = 1.45 and 1.1 were used, respectively, because these yielded the most reasonable PMFs for Lys^+/Glu^-. Figure 2D (inset) shows that the expected repulsion is

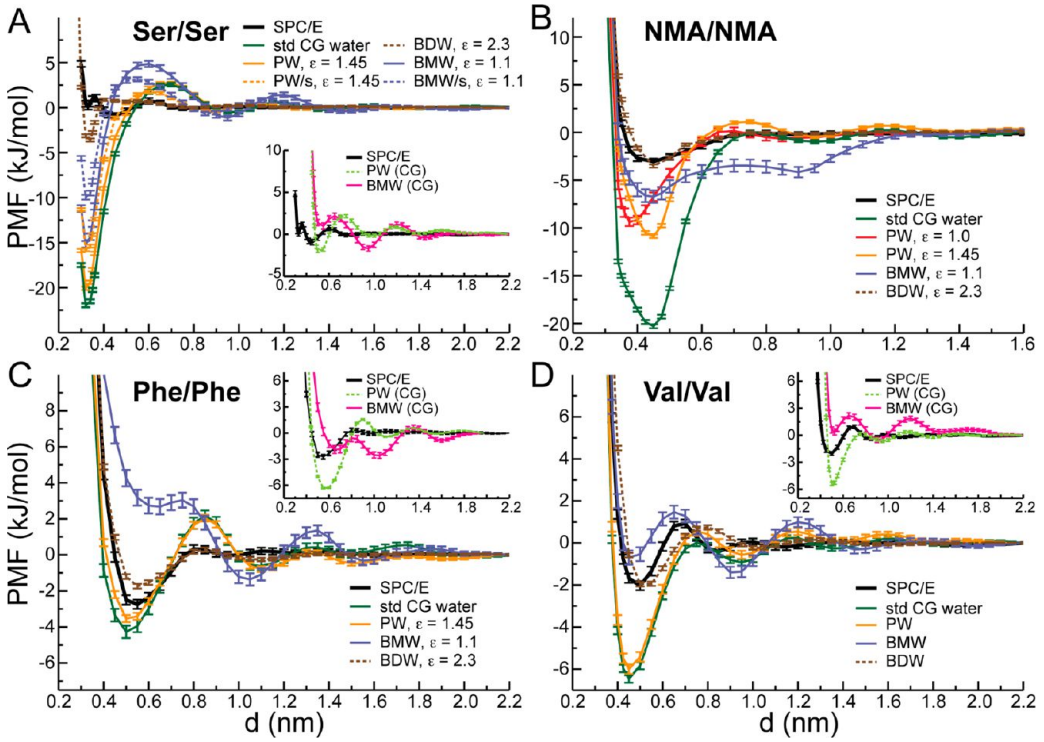

Figure 4. Potentials of mean force between uncharged molecules in water. (A) Atomistic Ser side chain analogues; (B) *n*-methylacetamide (NMA) molecules; (C) Phe and (D) Val side chain analogues. Fully AA and CG simulations are shown in the insets.

dx.doi.org/10.1021/jp311533p | J. Phys. Chem. B XXXX, XXX, XXX−XXX

observed in the fully atomistic and CG simulations. The hybrid AA/CG PMF in PW, however, displays an unphysical double minimum (Figure 2D, red curve). In this simulation, two coarse-grained Na^+ counterions were added to neutralize the charge of the simulation box. Closer analysis revealed that, at the distances corresponding to the minima, one of the two CG Na^+ counterions was binding to the atomistic Glu^-/Glu^- complex over extended time periods of several hundred picoseconds, which was not observed in SPC/E. To investigate this too strong counterion binding, the PMF was recalculated in the absence of counterions, i.e., for a system with net charge $-2e$ (dashed red curve). To test the effect of the net charged simulation box,[115−118] we also repeated the fully atomistic PMF calculations in the absence of counterions (dashed black curve). The PMFs from the AA simulations with and without counterions are comparable, with the counterions stabilizing the high negative charge density in the Glu^-/Glu^- complex by up to ca. 2 kJ/mol for close Glu^-/Glu^- distances. Thus, the net charge of the simulation system only rather weakly influences the PMFs and, in particular, does by itself not change the overall shape of the profiles. In the PW AA/CG system, the minimum at 0.8 nm vanishes in the absence of Na^+ counterions, but the one at 0.5 nm persists (compare dashed and solid red curves). A minimum is also observed in the AA/CG PMF in BMW (violet curves). The main conclusion is that the artificial minima in the AA/CG PMFs are not due to the presence or absence of counterions, but rather are due to an unphysical response of the CG solvent to the atomistic solutes. Repulsive PMFs can be obtained by increasing ε_r(AA−CG) (data not shown). However, this led to a strong overstabilization of like/unlike charge ion pairs, as described above. Similar binding of ions of like charge is expected not only for the Glu^-/Glu^- pair, but also for other species. Although not systematically investigated here, this effect is probably the worse the larger the magnitude and the more localized the charge.

Ser/Ser. Figure 4A shows the PMFs between two atomistic Ser side chain analogues (methanol molecules). The fully atomistic PMF (black curve) displays two minima at short distances and a very shallow barrier at 0.6 nm (+0.8 kJ/mol); see also Table S1 in the Supporting Information. The first minimum in the PMFs from the simulations at the fully CG level (Figure 4A, inset; green and magenta for PW and BMW, respectively) is located at a slightly too large distance. In PW, the minimum is somewhat too deep, whereas in BMW, it is only a local minimum that is even higher in energy than the dissociated state. The PMFs from the hybrid AA/CG simulations have deep minima at 0.325 nm, which are separated from the dissociated state by a barrier. The free energies of the minima are −20.1, −15.1, and −22.0 kJ/mol in PW, BMW, and standard MARTINI water, respectively. The height of the desolvation barrier depends on the water model and varies from +2.5 kJ/mol in standard MARTINI water to +5.0 kJ/mol in BMW. Motivated by the small size of the Ser side chain, we attempted to fine-tune the PMFs by changing the LJ parameters between the virtual CG sites and the CG water. The LJ interaction between the CG virtual site (MARTINI particle type P_1), located at the center of mass of the atomistic Ser particles, and the water beads was changed to a small-type MARTINI interaction; i.e., the radius σ_{LJ} was reduced from 0.47 to 0.43 nm, and the well depth ε_{LJ} was scaled by 75%.[49] These changes shifted the energies of the minimum and energy barrier by ca. +5 and −2 kJ/mol, respectively (dashed orange and violet curves in Figure 4A), bringing the AA/CG PMFs closer to the fully atomistic ones. Interestingly, the PMF obtained with the AA/CG model of Riniker et al.[54,56] has a shallow minimum at −3.6 kJ/mol and a very low barrier (dashed brown curve), in agreement with the fully atomistic PMF.

NMA/NMA. The PMFs between two NMA (*n*-methylacetamide) molecules are shown in Figure 4B. The fully atomistic PMF (black curve) has a shallow minimum around 0.45 nm (−3.0 kJ/mol). As discussed below, fully CG PMFs were not calculated due to the dependence of the backbone bead type on the secondary structure in the MARTINI model. The hybrid AA/CG PMF in PW (red curve) has a low-energy minimum at 0.45 nm (−10.8 kJ/mol) and a barrier at 0.75 nm (+1.0 kJ/mol). As opposed to Ser/Ser, where the PMFs in PW and BMW are quite similar (Figure 4A), for NMA, the PMF in BMW (violet curve) displays a very broad minimum and a long-ranged attractive tail up to a distance of about 0.9 nm. The missing dielectric screening in standard (Lennard-Jones) MARTINI water leads to a strong attraction (green curve), although the effect is less strong than for the ionic species (see above), as expected. The PMF obtained from hybrid simulations with the BDW model (dashed brown curve) quite closely agrees with the fully atomistic PMF.

In the MARTINI CG force field, the particle type of the amino acid backbone beads depends on the secondary structure.[70] We chose an N_0 type bead for the CG virtual site on NMA, an intermediate polarity that is commonly used for the backbone of α-helices. Although the choice of a different bead type would slightly change the PMFs, the basic features remain largely unaffected. It is desirable to overcome the limitation of secondary structure dependent bead types for simulations in which secondary structure changes occur; however, this is beyond the scope of this work.

Phe/Phe. Figure 4C shows the PMFs between two toluene molecules (representing Phe side chains). The fully atomistic PMF in SPC/E (inset, black curve) has a minimum at 0.55 nm (−2.7 kJ/mol) and a low-energy barrier at 0.8 nm (+0.3 kJ/mol). This PMF is very similar to the benzene−benzene PMF reported by Villa and co-workers.[119] The PMFs from the fully CG simulations are also shown in the inset (note that toluene and benzene are identical at the CG-MARTINI level). The PMF in PW (green) has a slightly too deep minimum at the correct distance of 0.55 nm (−6.3 kJ/mol). A barrier at 0.9 nm (+1.5 kJ/mol) separates it from the secondary minima. In BMW (magenta), however, the contact minimum has a higher energy than the secondary minima, similar to the molecule pairs described above. The first minimum in the PMF from the hybrid AA/CG simulations in PW (Figure 4C, orange curve) quite closely matches the one in the fully atomistic PMF. The minimum is slightly lower (−3.5 kJ/mol) and the barrier slightly higher than in the atomistic case due to the granularity of the water model. For apolar solutes such as Phe, ε_r(AA−CG) does not matter much, and the PMF in standard MARTINI water (green) is thus very similar to the one in PW. The PMF from the hybrid AA/CG simulations in BMW (violet) is similar to the fully CG PMF in that the first minimum is too high in energy. The minimum obtained with the BDW model is at −1.75 kJ/mol (dashed brown curve). Interestingly, despite the granularity of this water model (representing five atomistic water molecules), the desolvation energy barriers are as low as in atomistic solvent. Similarly low energy barriers with BDW were also observed for Ser/Ser and NMA/NMA; see above.

dx.doi.org/10.1021/jp311533p | J. Phys. Chem. B XXXX, XXX, XXX−XXX

Table 1. Solvation Free Enthalpies[a]

	ΔG_{aq}(AA/CG) PW/BMW	ΔG_{aq}(CG) PW/BMW	ΔG_{aq}(ex)	ΔG_{bu}(AA/CG) PW/BMW	ΔG_{bu}(CG) PW/BMW	ΔG_{ch}(ex)	$\Delta\Delta G$(AA/CG) PW/BMW	$\Delta\Delta G$(CG) PW/BMW	$\Delta\Delta G$(ex)
Asn	−47.5/−59.8	−24.5/−21.1	−40.5	+2.2	+2.0	−12.7	−49.7/−62.0	−26.5/−23.1	−27.8
Cys	−2.7/−0.2	−0.1/+2.4	−5.2	−7.1	−7.2	−10.5	+4.4/+6.9	+7.1/+9.6	+5.3
Gln	−41.6/−71.6	−18.7/−15.0	−39.2	+2.2	+2.0	−16.1	−43.8/−73.8	−20.7/−17.0	−23.1
Ile	+10.9/+11.1	+10.6/+10.0	+9.0	−11.0	−10.8	−11.6	+21.9/+22.1	+21.4/+20.8	+20.6
Leu	+10.9/+11.1	+10.6/+10.0	+9.5	−11.0	−10.8	−11.0	+21.9/+22.1	+21.4/+20.8	+20.5
Met	−7.6/−11.8	−0.1/+2.4	−6.2	−7.3	−7.2	−16.0	−0.3/−4.5	+7.1/+9.6	+10.2
Phe	−19.8/−6.8	−16.3/−3.3	−3.2	−38.8/−31.9	−37.0/−29.4	−15.6	+19.0/+25.1	+20.7/+26.1	+12.4
Ser	−18.9/−16.5	−13.5/−11.3	−21.2	−4.0	−3.9	−7.0	−14.9/−12.5	−9.6/−7.4	−14.2
Thr	−20.3/−22.1	−13.5/−11.3	−20.4	−4.0	−3.9	−9.7	−16.3/−18.1	−9.6/−7.4	−10.7
Trp	−52.5/−34.3	−41.3/−20.5	−24.6	−49.5/−39.5	−47.8/−38.7	−34.4	−3.0/+5.2	+6.5/+18.2	+9.8
Tyr	−37.0/−27.7	−32.2/−16.7	−25.6	−34.1/−27.1	−33.4/-26.7	−25.0	−2.9/−0.6	+1.2/+10.0	−0.6
Val	+7.2/+8.0	+7.5/+7.9	+8.3	−10.7	−11.1	−8.6	+17.9/+18.7	+18.6/+19.0	+16.9

[a]All values in kJ/mol. Statistical errors are <2 kJ/mol. In the hybrid AA/CG simulations in water, ε_r(AA−CG) = 1.45 and 1.1 were use for PW and BMW, respectively. Abbreviations: aq = water; ex = experiments by Radzicka and co-workers;[120] bu = butane; ch = cyclohexane.

Val/Val. Figure 4D shows the PMFs between two Val side chain analogues (propane molecules). The fully atomistic Val/Val PMF (inset, black curve) is similar to Phe/Phe (Figure 4C), in terms of both the locations and relative free energies of the minima and maxima. As for Phe/Phe, the PMFs obtained at the fully CG level are different in PW (green) and in BMW (magenta). In PW, the first minimum is energetically too low compared to the fully AA level, whereas in BMW it is again too high in energy relative to the solvent-separated minima. The contact minima in the PMFs from the hybrid AA/CG simulations in PW (Figure 4D, orange curve) and in standard MARTINI water (green) are too deep compared to the atomistic level. These two PMFs are the same (within statistical errors) in this case, since united-atom aliphatic CH_n groups do not carry a partial charge in the Gromos 53A6 force field. The hybrid AA/CG PMF in BMW (violet) again has a too high energy of the first minimum. The AA/CG PMF in BDW water (dashed brown curve) again quite closely matches the fully atomistic one.

To summarize the results from the PMF calculations, the investigated electrostatic coupling AA/CG schemes did not provide a reasonable energetic description of the dimerization of charged molecules in water. For polar molecules, the situation is slightly better, in particular with the BDW water model,[54−56] although this AA/CG model most severely overestimated the binding of the Lys^+/Glu^- pair (by ca. 150 kJ/mol). For the investigated apolar molecules, AA/CG PMFs can be close to the fully AA level. In BMW water, the relative free energy of the contact minimum is higher than of the solvent-separated minima. This qualitative discrepancy with the atomistic PMFs was observed not only in the AA/CG simulations with the BMW model, but also at the fully CG-BMW level.

Free Enthalpies of Solvation. In Table 1 and Figure 5, the calculated free enthalpies of solvation of uncharged amino acid side chain analogues in CG water and CG butane are compared to experimental data.[120] The mean absolute error (with respect to experiment) of the partitioning free enthalpy, $\Delta\Delta G$, between water and apolar solvent is 7.1 and 11.0 kJ/mol for the hybrid simulations with the PW and BMW models, respectively. The corresponding errors from the fully CG simulations are 2.7 and 5.1 kJ/mol in PW and BMW, respectively. When interpreting these errors, one has to take into account that the experimental data in apolar solvent were measured not in butane but in cyclohexane; however, the difference can be expected to be small. The solvation free enthalpies from the fully CG models reported in Table 1 quantitatively agree with published data.[72,74]

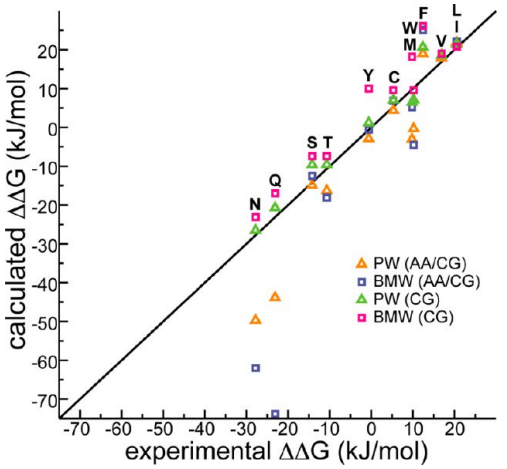

Figure 5. Calculated versus experimental partitioning free enthalpies.

Notably, the accuracy of the partitioning free enthalpies, $\Delta\Delta G$, predicted by the fully coarse-grained PW MARTINI model is comparable to fully atomistic models,[95] although this partly results from compensation of errors (see below). The accuracy of the hybrid AA/CG models cannot rival that of the fully AA or CG models, although significantly better results are obtained for apolar solutes than for polar solutes. Compared to the fully CG models, the hybrid AA/CG model tends to yield larger absolute solvation free enthalpies of polar solutes in water. This can be explained by the additive AA/CG coupling scheme: Solute−solvent Coulomb interactions are added to the CG Lennard-Jones interactions, which, owing to the CG parametrization, already implicitly include some electrostatic contribution. An additional difference between measured and calculated partitioning free enthalpies is due to the entropy loss inherent with removing degrees of freedom upon coarse-graining.[121] This effect is less pronounced at the fully CG level, where an entropic contribution is implicitly incorporated into the CG potentials.

A closer look at some individual molecules can provide deeper insights into the partitioning behavior. Two illustrative examples are the polar Asn and Gln side chains. The AA/CG

dx.doi.org/10.1021/jp311533p | J. Phys. Chem. B XXXX, XXX, XXX−XXX

simulations yielded free enthalpies of hydration of −47.5 and −41.6 kJ/mol for Asn and Gln in PW, respectively, in favorable agreement with experiment.[120] In apolar butane solvent, however, the ΔG of +2.2 kJ/mol is considerably too positive compared to experiment (−12.7 and −16.1 kJ/mol for Asn and Gln, respectively), resulting in large errors in $\Delta\Delta G$. At the fully CG level, errors compensate, since the solvation free enthalpies in both water and butane are too positive (ΔG_{bu}(AA/CG) and ΔG_{bu}(CG) are the same within the statistical errors, since there are no electrostatic solute−solvent interactions in this case). Noticeable are also the very negative AA/CG solvation free enthalpies of Asn and, even more so, Gln in BMW. These are due to the very strong electrostatic interactions between the solutes and the large charges on BMW (+1e and −2e on the satellite and central particles, respectively).

Aromatic side chains are also worth discussion. Phe is apolar, and thus the free enthalpies from the AA/CG simulations and the fully CG simulations are similar. Solvation of Phe in PW is too favorable compared to experiment. Although this is compensated by a too negative ΔG also in apolar solvent, the latter is much too favorable in this case, and the resulting $\Delta\Delta G$ thus deviates from experiment by 8 kJ/mol. To improve this, in the new MARTINI v.2.2 parameter set[110] the CG particle type of benzene (and thus Phe) was changed from SC4 to SC5, yielding a $\Delta\Delta G$ of +10 kJ/mol that is in good agreement with experiment. In the BMW-MARTINI model,[74] the LJ interaction between the SC4-type CG beads comprising the Phe side chain and the BMW beads is scaled by 71% compared to the original MARTINI model. This reduction brings the free enthalpy of hydration closer to the experimental value. However, since the LJ interaction between Phe and the C1-type particles of the CG butane is scaled by only 90% in BMW-MARTINI,[74] error compensation is worse than in PW, and the deviation of $\Delta\Delta G$ from experiment is rather large (ca. 14 kJ/mol). These effects, which are also observed for the other aromatic side chains Trp and Tyr (see Table 1), explain why, in terms of partitioning free enthalpies $\Delta\Delta G$, PW-MARTINI agrees more favorably with experiment than BMW-MARTINI does (Figure 5).

Small Soluble Proteins. The next test for our AA/CG hybrid model was to investigate small soluble proteins in water. For this aim, the GCN4-p1 peptide and ubiquitin were chosen as test systems. Figure 6A compares the secondary structure of the GCN peptide during the hybrid AA/CG simulation in PW (upper panel) and the fully atomistic simulation in SPC water (lower panel). In the hybrid simulation GCN adopted a very stable α-helical structure, in particular the N-terminus, whereas in SPC water both α- and π-helices were observed, with several structural transitions between them on the 100-ns time scale. Close inspection of the trajectories revealed that, in the hybrid AA/CG simulation, a salt bridge was established between Glu22 and Arg25, which was stable throughout the entire 100-ns simulation time (Figure 6B, green and blue curves). In addition, a hydrogen bond formed between Tyr17 and Glu22, which also persisted throughout the entire simulation. These overly stable interactions, which locked the peptide in the α-helical conformation, were also observed in an additional 100-ns hybrid AA/CG simulation of the GCN peptide in BDW, i.e., the model of Riniker and co-workers[56] (data not shown). By contrast, in SPC water no such stable interactions were observed (Figure 6B, black and red curves). Although transient salt bridges and hydrogen bonds between the respective side chains were also observed in this fully atomistic simulation,

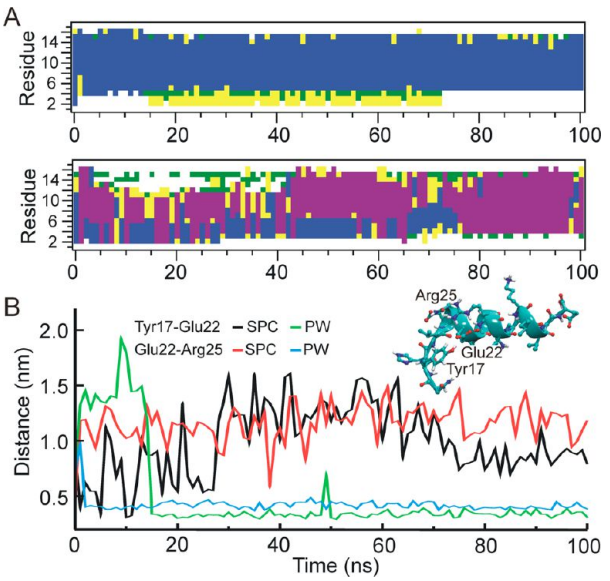

Figure 6. MD simulations of atomistic GCN peptide. (A) Secondary structure in PW-CG water with ε_r(AA−CG) = 1.45 (upper panel) and in SPC water (lower panel). Color code: α-helix, blue; π-helix, violet; β-sheet, red; turn, yellow; bend, green; coil, white. Secondary structure was assigned using DSSP.[124] (B) Distances between the indicated residues in SPC versus PW-CG water. The atoms chosen to measure the distances were the oxygen atom of the Tyr side chain and the terminal carbon atoms of the Glu and Arg side chains, respectively.

none of the individual interactions was established for extended periods of time, hence allowing for a much higher structural flexibility. The observed transitions between α- and π-helical conformations agree with other all-atom simulation results.[122,123]

For ubiquitin, Figure 7 shows that, during the hybrid MD simulation in PW water with ε_r(AA−CG) = 1.45, the protein

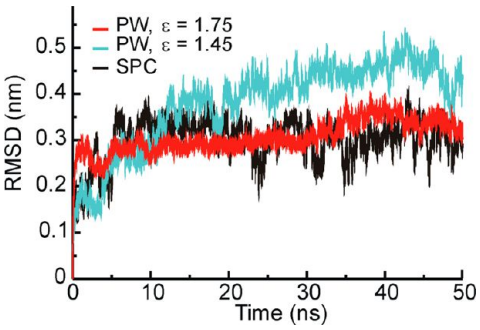

Figure 7. Root-mean-square deviation (rmsd) of Cα atoms of ubiquitin with respect to the starting structure. The rmsd's from the hybrid AA/CG simulations in PW-CG water are shown in red and cyan for ε_r(AA−CG) = 1.75 and 1.45, respectively; the fully atomistic simulation in SPC water is in black.

deviated from its starting structure, as evidenced by a Cα root-mean-square deviation (rmsd) larger than 0.4 nm after 10−20 ns (cyan curve). Interestingly, using ε_r = 1.75 increases the structural stability of the protein: The Cα rmsd is 0.3 nm after 50 ns (red curve), similar to the structural deviation observed during the fully atomistic simulation (black curve). In addition to the simulations in PW water, we also carried out the respective hybrid AA/CG simulations using the standard (uncharged) MARTINI water model. Since the water cannot

dx.doi.org/10.1021/jp311533p | J. Phys. Chem. B XXXX, XXX, XXX−XXX

explicitly screen the AA−AA electrostatic interactions in this case, a uniform dielectric permittivity, ε_r, was used, which was systematically varied between 1 and 78. A total of 14 simulations with different values of ε_r were carried out. In all cases, a rapid (<10 ns) increase of the Cα rmsd concomitant with a loss of secondary structure was observed (data not shown), highlighting that a simple uniform dielectric permittivity is not appropriate in the context of our hybrid AA/CG model.

To obtain a more detailed view, the secondary structure was analyzed. Figure 8 shows that the structural elements of

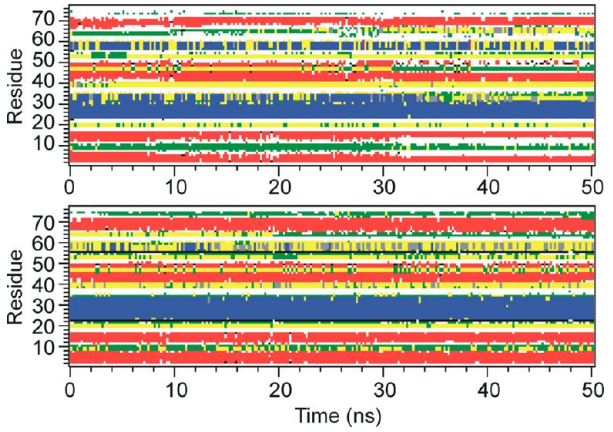

Figure 8. Secondary structure of ubiquitin in PW-CG water with ε_r(AA−CG) = 1.75 (upper panel) and in SPC water (lower panel). The color code is the same as in Figure 6.

ubiquitin are reasonably well preserved during the hybrid simulation in PW (upper panel) compared to the simulation in SPC (lower panel), although in particular the N-terminal β-sheets appear less stable during the last 20 ns. This structural stability may be considered surprising in light of the above PMF and partitioning data. Close inspection of the simulation revealed that charged and polar residues on the protein surface formed overly stable salt bridges and hydrogens bonds that, after having formed at the beginning, did not break up again in the course of the simulations, similar to the too stable interactions observed for the GCN peptide; see above. Similar results were obtained with the hybrid AA/CG model suggested by Riniker and co-workers[125] (data not shown). These interactions would need to break up to allow for structural rearrangements, and hence the observed stability can be explained by kinetic trapping of the protein structure in a too deep energy minimum.

Membrane-Embedded Systems. Next, we applied our hybrid AA/CG model to a transmembrane segment that is completely buried in the lipid bilayer, i.e., one that does not have water-soluble parts. To this aim, we simulated an α-helical WALP23 peptide embedded in a CG DPPC bilayer. Simulations with the PW, BMW, and standard MARTINI water models, respectively, were carried out, and the secondary structure of the peptide was analyzed. Figure 9A shows the final snapshot (after 60 ns) from the simulation of the WALP23 peptide in PW. The α-helix was very stable during the simulations, irrespective of the water model used, with an average helicity (averaged of the last 40 ns of the simulation) of >85% for all three CG water models.

Finally, a C-terminus deleted MscL embedded in a DOPC bilayer was simulated; see Figure 9B. Hybrid AA/CG simulations were carried out using CG DOPC with the PW or standard MARTINI water models, both with and without the addition of CG counterions. As a reference, we also carried out a fully atomistic simulation of the same system (using the Gromos 54A7 parameter set[123] for MscL and DOPC, and the SPC water model). Contrary to WALP23, the C-terminus deleted MscL has a number of water-accessible residues. In addition, water can enter the channel pore. In PW, both with and without CG ions, the overall structure was largely maintained, comparable to the fully atomistic simulation (Figure 10). As expected from the PMFs (Figure 2), in the simulation with mobile counterions, the CG ions bonded to strongly to charged AA side chains, and the zwitterionic DOPC lipids stuck too much to the protein. In standard MARTINI water, both with and without CG ions, a rapid loss of secondary structure was observed during the first few nanoseconds of the simulations (data not shown), starting with residues that are exposed to water.

General Discussion. We found that the applied hybrid AA/CG models can yield reasonable results for apolar solutes in water and for solutes in an apolar environment. Charged and

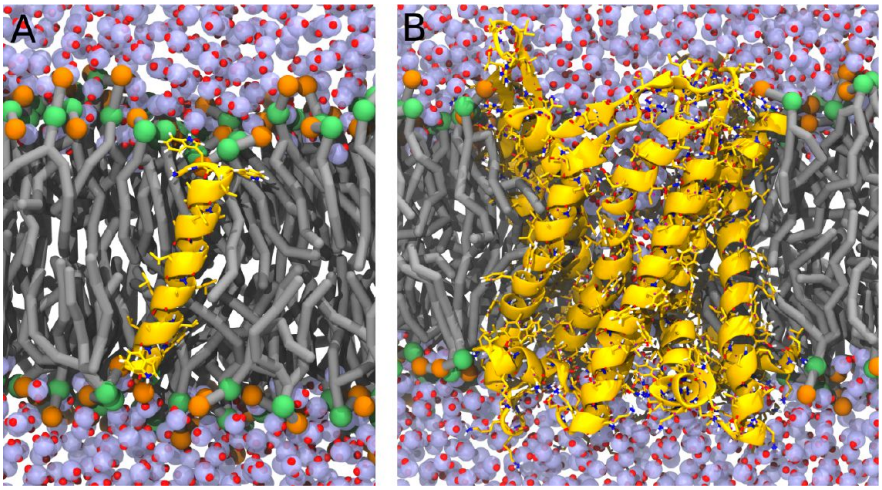

Figure 9. Hybrid AA/CG simulations of membrane-embedded systems. Snapshots from simulation of (A) atomistic WALP23 embedded in a CG DPPC bilayer, and (B) truncated MscL in DOPC.

dx.doi.org/10.1021/jp311533p | J. Phys. Chem. B XXXX, XXX, XXX−XXX

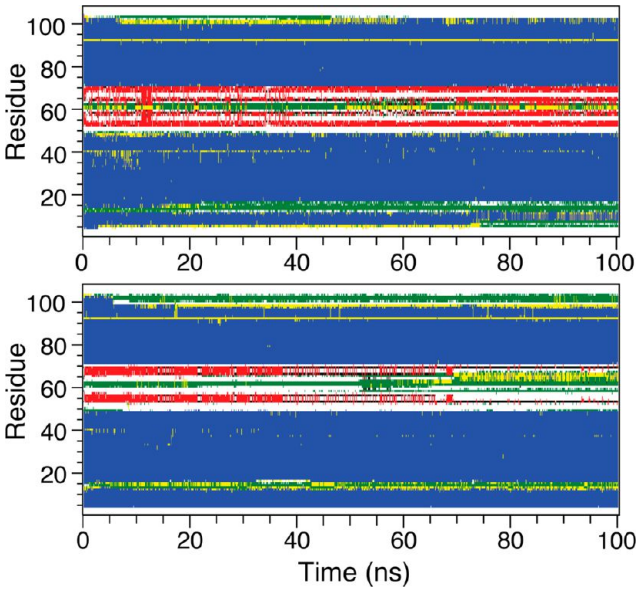

Figure 10. Secondary structure of C-terminus truncated MscL in a DOPC bilayer during hybrid AA/CG simulation in CG bilayer solvated with PW-CG water (upper panel) and in fully atomistic simulation (lower panel). The secondary structure is shown only for one subunit of the pentameric MscL; the respective plots for the other subunits are similar.

polar solutes in water, however, still represent a major challenge. This may be due to the nature of the CG water models used: Just like other CG water models,[55,80,81] the polarizable PW[72] and BMW[73] models were parametrized to reproduce properties of bulk water, in particular the density and the relative static dielectric permittivity. However, by construction, these CG models cannot provide a realistic physical description of local, short-ranged interactions that play a dominant role close to interfaces (or molecular surfaces), such as hydrogen bonding and first solvation shell effects. In this respect, CG and AA models may be considered inherently incompatible. A possible remedy could be to introduce explicit hydrogen bonding energy terms, which however would require extensive (re)parametrization.

The structure of the studied atomistic proteins (or polypeptides) embedded in a polarizable MARTINI CG environment was largely preserved on the 50−100 ns time scale, despite the observed profound differences between the hybrid simulations and the fully atomistic simulations in terms of the PMFs and partitioning free enthalpies, in particular for the charged/polar species. Although we only studied a handful of different systems, and we thus cannot generalize for all possible protein structures, the too deep minima and too high barriers observed in the side chain−side chain PMFs as well as the too stable salt bridges and hydrogen bonds observed in the protein simulations strongly suggest that the structures are trapped in local minima, and deviations would thus occur only on much longer time scales. This overstabilization results from an increased stability of protein−protein contacts in the absence of the possibility to form hydrogen bonds to the solvent.

One of the major aims of multiscale modeling is to reduce computational cost. Using the WALP23/DPPC system as a benchmark, we found that the simulations with our hybrid AA/CG model were faster by factors of 8 and 12 in PW and standard MARTINI water, respectively, compared to a simulation of the same system at the fully AA level (these simulations were carried out on four CPU cores using MPI parallelization, with the same settings for the nonbonded interactions to ensure comparability). Multiple time step integration would yield a substantial additional gain, since the CG degrees of freedom need to be updated less frequently than the atomistic ones. The computational efficiency of such hybrid simulations can be compared to implicit solvation models. However, for many systems, an explicit particle-based description is desirable, e.g., for (multicomponent) lipid membranes, which are characterized by a heterogeneous distribution of functional groups. An obvious approach for improving the behavior of proteins or other solutes in hybrid simulations is to introduce layers of atomistic solvent around the solute, thus shifting the AA/CG interface away from the molecule of interest.[126] Riniker and co-workers found that a water layer of thickness 0.8 nm suffices for this purpose.[125] However, such an approach significantly reduces the achievable computational speedup with respect to fully atomistic simulations, especially when minimal-volume boxes are employed.[127] In our view, for a hybrid model to be really useful for and widely accepted by the scientific community, it should provide a significant speedup with respect to the corresponding fully atomistic simulation to justify the inherent and probably unavoidable loss in accuracy. Such an efficiency gain would ensure that the model allows one to explore time and length scales that are out of reach for atomistic simulations.

CONCLUSIONS

In this study, we derived and critically tested efficient hybrid AA/CG models for biomolecular simulations that explicitly incorporate electrostatic interactions between AA and CG subsystems. Atomistic solutes, described with different parameter sets of the Gromos force field,[75−77] were solvated in a CG environment that was modeled with the MARTINI force field. To enact electrostatic coupling between AA and CG subsystems, we employed two recently developed MARTINI water models with explicit electrostatic interactions, the polarizable water (PW) model[72] and the BMW model.[73] The strength of the electrostatic coupling between AA and CG was adjusted through the relative dielectric permittivity ε_r(AA−CG). In addition, the CG dipole water model of Riniker and co-workers[54−56] was used. Potential of mean force (PMF) calculations revealed significant differences between the hybrid simulations and the fully AA or CG simulations for pairs of charged molecules in water. For the studied systems, a satisfactory agreement between atomistic and hybrid PMFs could not be obtained by varying ε_r(AA−CG). However, for apolar solutes, and partly also for polar ones, the hybrid AA/CG PMFs were more similar to the fully atomistic results. The hybrid AA/CG partitioning free enthalpies of uncharged amino acid side chains between butane and water deviate more strongly from experiment than both the fully atomistic and CG results, with better agreement for apolar than for polar side chains.

Comparing the PW-MARTINI and BMW-MARTINI models at the fully CG level revealed that the side chain−side chain PMFs in PW are similar to the fully atomistic simulations. The BMW model yielded contact minima that are too high in energy compared to the solvent-separated minima for all side chain pairs studied. The partitioning free enthalpies obtained with the PW model at the fully CG level agree almost as well with experimental data as fully atomistic models.

dx.doi.org/10.1021/jp311533p | J. Phys. Chem. B XXXX, XXX, XXX−XXX

Despite the described limitations of the hybrid models, the structures of atomistic solutes embedded in a CG environment, such as the GCN peptide and ubiquitin solvated in polarizable MARTINI CG water, a single transmembrane α-helix embedded in a CG DPPC bilayer, and a truncated mechanosensitive channel in a CG DOPC bilayer, were largely maintained during 50−100 ns AA/CG MD simulations. These results reflect an overstabilization due to too deep energy minima and highlight the importance of analyzing not only structural but also thermodynamic data when evaluating a model. In conclusion, the aim of this work was not to put forward a complete and ready-to-use AA/CG model for biomolecular simulations of various systems, but to highlight challenges that will need to be addressed in the future when developing hybrid models that can ultimately rival the established atomistic simulations.

■ ASSOCIATED CONTENT

Supporting Information

Table with maxima and minima of PMFs. This material is available free of charge via the Internet at http://pubs.acs.org.

■ AUTHOR INFORMATION

Corresponding Author

*E-mail: schaefer@chemie.uni-frankfurt.de.

Author Contributions

T.A.W. developed the software for simulation setup and interpreted data. H.I.I. and M.P. acquired and interpreted data. S.J.M. interpreted data and designed research. L.V.S. designed research, implemented the model, and acquired and interpreted data. L.V.S. wrote the article, together with the other authors.

T.A.W. and H.I.I. contributed equally to this work.

Notes

The authors declare no competing financial interest.

■ ACKNOWLEDGMENTS

We thank Djurre de Jong for providing the all-atom topologies of the side chain analogues and Bernd Ensing, Martti Louhivuori, and Christine Peter for discussions and carefully reading the manuscript. This work was supported by the Deutsche Forschungsgemeinschaft (SFB 807 and Emmy Noether grant SCHA1574/3-1) and by The Netherlands Organisation for Scientific Research (NWO), Top Grant 700.57.303.

■ REFERENCES

(1) Karplus, M.; McCammon, J. A. *Nat. Struct. Biol.* **2002**, *9*, 646−652.

(2) Gumbart, J.; Wang, Y.; Aksimentiev, A.; Tajkhorshid, E.; Schulten, K. *Curr. Opin. Struct. Biol.* **2005**, *15*, 423−431.

(3) Marrink, S. J.; de Vries, A. H.; Tieleman, D. P. *Biochim. Biophys. Acta* **2009**, *1788*, 149−168.

(4) van Gunsteren, W. F.; Bakowies, D.; Baron, R.; Chandrasekhar, I.; Christen, M.; Daura, X.; Gee, P.; Geerke, D. P.; Glattli, A.; Hünenberger, P. H.; Kastenholz, M. A.; Ostenbrink, C.; Schenk, M.; Trzesniak, D.; van der Vegt, N. F. A.; Yu, H. B. *Angew. Chem., Int. Ed.* **2006**, *45*, 4064−4092.

(5) Voth, G. A. *Coarse-Graining of Condensed Phase and Biomolecular Systems*; CRC Press/Taylor and Francis: Boca Raton, FL, 2009.

(6) Nielsen, S. O.; Lopez, C. F.; Srinivas, G.; Klein, M. L. *J. Phys.: Condens. Matter* **2004**, *16*, R481−R512.

(7) Tozzini, V. *Curr. Opin. Struct. Biol.* **2005**, *15*, 144−150.

(8) Smit, B.; Hilbers, P. A. J.; Esselink, K.; Rupert, L. A. M.; van Os, N. M.; Schlijper, A. G. *Nature* **1990**, *348*, 624−625.

(9) Shelley, J. C.; Shelley, M. Y.; Reeder, R. C.; Bandyopadhyay, S.; Klein, M. L. *J. Phys. Chem. B* **2001**, *105*, 4464−4470.

(10) Goetz, R.; Lipowsky, R. *J. Chem. Phys.* **1998**, *108*, 7397−7409.

(11) Marrink, S. J.; de Vries, A. H.; Mark, A. E. *J. Phys. Chem. B* **2004**, *108*, 750−760.

(12) Izvekov, S.; Voth, G. A. *J. Phys. Chem. B* **2005**, *109*, 2469−2473.

(13) Onuchic, J. N.; Wolynes, P. G. *Curr. Opin. Struct. Biol.* **2004**, *14*, 70−75.

(14) Chebaro, Y.; Pasquali, S.; Derreumaux, P. *J. Phys. Chem. B* **2012**, *116*, 8741−8752.

(15) Shih, A. Y.; Arkhipov, A. S.; Freddolino, P. L.; Schulten, K. *J. Phys. Chem. B* **2006**, *110*, 3674−3684.

(16) Bond, P. J.; Sansom, M. S. P. *J. Am. Chem. Soc.* **2006**, *128*, 2697−2704.

(17) Fuhrmans, M.; Marrink, S. J. *J. Am. Chem. Soc.* **2012**, *134*, 1543−1552.

(18) Periole, X.; Huber, T.; Marrink, S. J.; Sakmar, T. P. *J. Am. Chem. Soc.* **2007**, *129*, 10126−10132.

(19) Reynwar, B. J.; Illya, G.; Harmandaris, V. A.; Muller, M. M.; Kremer, K.; Deserno, M. *Nature* **2007**, *447*, 461−464.

(20) Reynwar, B. J.; Deserno, M. *Biointerphases* **2008**, *3*, FA117−FA124.

(21) Schmidt, U.; Guigas, G.; Weiss, M. *Phys. Rev. Lett.* **2008**, *101*, 128104.

(22) Sengupta, D.; Marrink, S. J. *Phys. Chem. Chem. Phys.* **2010**, *12*, 12987−12996.

(23) Schäfer, L. V.; de Jong, D. H.; Holt, A.; Rzepiela, A. J.; de Vries, A. H.; Poolman, B.; Killian, J. A.; Marrink, S. J. *Proc. Natl. Acad. Sci. U.S.A.* **2011**, *108*, 1343−1348.

(24) Morozova, D.; Guigas, G.; Weiss, M. *PLoS Comput. Biol.* **2011**, *7*, e1002067.

(25) Bogaart, G. v. d.; Meyenberg, K.; Risselada, H. J.; Amin, H.; Willig, K. I.; Hubrich, B. E.; Dier, M.; Hell, S. W.; Grubmüller, H.; Diederichsen, U.; Jahn, R. *Nature* **2011**, *479*, 552−555.

(26) Parton, D. L.; Klingelhoefer, J. W.; Sansom, M. S. P. *Biophys. J.* **2011**, *101*, 691−699.

(27) Domanski, J.; Marrink, S. J.; Schäfer, L. V. *Biochim. Biophys. Acta, Biomembr.* **2012**, *1818*, 984−994.

(28) Zacharias, M. *Protein Sci.* **2003**, *12*, 1271−1282.

(29) Ayton, G. S.; Noid, W. G.; Voth, G. A. *Curr. Opin. Struct. Biol.* **2007**, *17*, 192−198.

(30) Peter, C.; Kremer, K. *Soft Matter* **2009**, *5*, 4357−4366.

(31) Tschöp, W.; Kremer, K.; Hahn, O.; Batoulis, J.; Bürger, T. *Acta Polym.* **1998**, *49*, 75−79.

(32) Milano, G.; Müller-Plathe, F. *J. Phys. Chem. B* **2005**, *109*, 18609−18619.

(33) Hess, B.; Leon, S.; van der Vegt, N.; Kremer, K. *Soft Matter* **2006**, *2*, 409−414.

(34) Harmandaris, V. A.; Adhikari, N. P.; van der Vegt, N. F. A.; Kremer, K. *Macromolecules* **2006**, *39*, 6708−6719.

(35) Heath, A. P.; Kavraki, L. E.; Clementi, C. *Proteins: Struct., Funct., Bioinf.* **2007**, *68*, 646−661.

(36) Shih, A. Y.; Freddolino, P. L.; Sligar, S. G.; Schulten, K. *Nano Lett.* **2007**, *7*, 1692−1696.

(37) Villa, A.; Peter, C.; van der Vegt, N. F. A. *Phys. Chem. Chem. Phys.* **2009**, *11*, 2077−2086.

(38) Rzepiela, A. J.; Schäfer, L. V.; Goga, N.; Risselada, H. J.; de Vries, A. H.; Marrink, S. J. *J. Comput. Chem.* **2010**, *31*, 1333−1343.

(39) Stansfeld, P. J.; Sansom, M. S. P. *J. Chem. Theory Comput.* **2011**, *7*, 1157−1166.

(40) Warshel, A. *Annu. Rev. Biophys. Biomol. Struct.* **2003**, *32*, 425−443.

(41) Lin, H.; Truhlar, D. G. *Theor. Chem. Acc.* **2007**, *117*, 185−199.

(42) Shi, Q.; Izvekov, S.; Voth, G. A. *J. Phys. Chem. B* **2006**, *110*, 15045−15048.

(43) Izvekov, S.; Voth, G. A. *J. Chem. Phys.* **2005**, *123*, 134105.

(44) Michel, J.; Orsi, M.; Essex, J. W. *J. Phys. Chem. B* **2008**, *112*, 657−660.
(45) Orsi, M.; Sanderson, W. E.; Essex, J. W. *J. Phys. Chem. B* **2009**, *113*, 12019−12029.
(46) Masella, M.; Borgis, D.; Cuniasse, P. *J. Comput. Chem.* **2011**, *32*, 2664−2678.
(47) Masella, M.; Borgis, D.; Cuniasse, P. *J. Comput. Chem.* **2008**, *29*, 1707−1724.
(48) Rzepiela, A. J.; Louhivuori, M.; Peter, C.; Marrink, S. J. *Phys. Chem. Chem. Phys.* **2011**, *13*, 10437−10448.
(49) Marrink, S. J.; Risselada, H. J.; Yefimov, S.; Tieleman, D. P.; de Vries, A. H. *J. Phys. Chem. B* **2007**, *111*, 7812−7824.
(50) Han, W.; Wan, C. K.; Jiang, F.; Wu, Y.-D. *J. Chem. Theory Comput.* **2010**, *6*, 3373−3389.
(51) Han, W.; Wan, C. K.; Wu, Y.-D. *J. Chem. Theory Comput.* **2010**, *6*, 3390−3402.
(52) Wan, C. K.; Han, W.; Wu, Y.-D. *J. Chem. Theory Comput.* **2012**, *8*, 300−313.
(53) Han, W.; Schulten, K. *J. Chem. Theory Comput.* **2012**, *8*, 4413−4424.
(54) Riniker, S.; van Gunsteren, W. F. *J. Chem. Phys.* **2012**, *137*, 044120.
(55) Riniker, S.; van Gunsteren, W. F. *J. Chem. Phys.* **2011**, *134*, 084110.
(56) Riniker, S.; Eichenberger, A. P.; van Gunsteren, W. F. *Eur. Biophys. J.* **2012**, *41*, 647−661.
(57) Neri, M.; Anselmi, C.; Cascalla, M.; Maritan, A.; Carloni, P. *Phys. Rev. Lett.* **2005**, *95*, 218102.
(58) Abrams, C. F. *J. Chem. Phys.* **2005**, *123*, 234101.
(59) Praprotnik, M.; Delle Site, L.; Kremer, K. *J. Chem. Phys.* **2005**, *123*, 224106.
(60) Ensing, B.; Nielsen, S. O.; Moore, P. B.; Klein, M. L.; Parrinello, M. *J. Chem. Theory Comput.* **2007**, *3*, 1100−1105.
(61) Heyden, A.; Truhlar, D. G. *J. Chem. Theory Comput.* **2008**, *4*, 217−221.
(62) Praprotnik, M.; Delle Site, L.; Kremer, K. *Annu. Rev. Phys. Chem.* **2008**, *59*, 545−571.
(63) Praprotnik, M.; Delle Site, L.; Kremer, K. *J. Chem. Phys.* **2007**, *126*, No. 134902.
(64) Nielsen, S. O.; Bulo, R. E.; Moore, P. B.; Ensing, B. *Phys. Chem. Chem. Phys.* **2010**, *12*, 12401−12414.
(65) Heyden, A.; Lin, H.; Truhlar, D. G. *J. Phys. Chem. B* **2007**, *111*, 2231−2241.
(66) Bulo, R. E.; Ensing, B.; Sikkema, J.; Visscher, L. *J. Chem. Theory Comput.* **2009**, *5*, 2212−2221.
(67) Christen, M.; van Gunsteren, W. F. *J. Chem. Phys.* **2006**, *124*, 1541061−1541067.
(68) Liu, P.; Voth, G. A. *J. Chem. Phys.* **2007**, *126*, 045106.
(69) Lyman, E.; Ytreberg, F. M.; Zuckerman, D. M. *Phys. Rev. Lett.* **2006**, *96*, 0281051.
(70) Monticelli, L.; Kandasamy, S. K.; Periole, X.; Larson, R. G.; Tieleman, D. P.; Marrink, S. J. *J. Chem. Theory Comput.* **2008**, *4*, 819−834.
(71) Lopez, C. A.; Rzepiela, A. J.; de Vries, A. H.; Dijkhuizen, L.; Hünenberger, P. H.; Marrink, S. J. *J. Chem. Theory Comput.* **2009**, *5*, 3195−3210.
(72) Yesylevskyy, S. O.; Schäfer, L. V.; Sengupta, D.; Marrink, S. J. *PLoS Comput. Biol.* **2010**, *6*, e1000810.
(73) Wu, Z.; Cui, Q.; Yethiraj, A. *J. Phys. Chem. B* **2010**, *114*, 10524−10529.
(74) Wu, Z.; Cui, Q.; Yethiraj, A. *J. Chem. Theory Comput.* **2011**, *7*, 3793−3802.
(75) Schuler, L. D.; van Gunsteren, W. F. *Mol. Simul.* **2000**, *25*, 301−319.
(76) Schuler, L. D.; Daura, X.; van Gunsteren, W. F. *J. Comput. Chem.* **2001**, *22*, 1205−1218.
(77) Oostenbrink, C.; Villa, A.; Mark, A. E.; van Gunsteren, W. F. *J. Comput. Chem.* **2004**, *25*, 1656−1676.
(78) Berendsen, H. J. C.; Grigera, J. R.; Straatsma, T. P. *J. Phys. Chem.* **1987**, *91*, 6269−6271.
(79) Neumann, M. *Mol. Phys.* **1983**, *50*, 841−858.
(80) Ha-Duong, T.; Basdevant, N.; Borgis, D. *Chem. Phys. Lett.* **2009**, *468*, 79−82.
(81) Darré, L.; Machado, M. R.; Dans, P. D.; Herrera, F. E.; Pantano, S. *J. Chem. Theory Comput.* **2010**, *6*, 3793−3807.
(82) Hess, B.; Kutzner, C.; van der Spoel, D.; Lindahl, E. *J. Chem. Theory Comput.* **2008**, *4*, 435−447.
(83) van Gunsteren, W. F.; Berendsen, H. J. C. *Mol. Simul.* **1988**, *1*, 173−185.
(84) Berendsen, H. J. C.; Postma, J. P. M.; van Gunsteren, W. F.; DiNola, A.; Haak, J. R. *J. Chem. Phys.* **1984**, *81*, 3684−3690.
(85) Hess, B. *J. Chem. Theory Comput.* **2008**, *4*, 116−122.
(86) Hess, B.; Dekker, H.; Berendsen, H. J. C.; Fraaije, J. G. E. M. *J. Comput. Chem.* **1997**, *18*, 1463−1472.
(87) Miyamoto, S.; Kollman, P. A. *J. Comput. Chem.* **1992**, *13*, 952−962.
(88) Hess, B.; Holm, C.; van der Vegt, N. F. A. *J. Chem. Phys.* **2006**, *124*, 164509.
(89) Hess, B. *J. Chem. Phys.* **2002**, *116*, 209−217.
(90) de Jong, D. H.; Schäfer, L. V.; de Vries, A. H.; Marrink, S. J.; Berendsen, H. J. C.; Grubmüller, H. *J. Comput. Chem.* **2011**, *32*, 1919−1928.
(91) Ouldridge, T. E.; Louis, A. A.; Doye, J. P. K. *J. Phys. Condens. Matter* **2012**, 104102.
(92) de Jong, D. H.; Periole, X.; Marrink, S. J. *J. Chem. Theory Comput.* **2012**, *8*, 1003−1014.
(93) Lindahl, E.; Hess, B.; van der Spoel, D. *J. Mol. Model.* **2001**, *7*, 306−317.
(94) Shirts, M. R.; Pitera, J. W.; Swope, W. C.; Pande, V. S. *J. Chem. Phys.* **2003**, *119*, 5740−5761.
(95) Hess, B.; van der Vegt, N. F. A. *J. Phys. Chem. B* **2006**, *110*, 17616−17626.
(96) Darden, T.; York, D.; Pedersen, L. *J. Chem. Phys.* **1993**, *98*, 10089−10092.
(97) Bennett, C. H. *J. Comput. Phys.* **1976**, *22*, 245−268.
(98) Steinmetz, M. O.; Jelesarov, I.; Matousek, W. M.; Honnappa, S.; Jahnke, W.; Missimer, J. H.; Frank, S.; Alexandrescu, A. T.; Kammerer, R. A. *Proc. Natl. Acad. Sci. U.S.A.* **2007**, *104*, 7062−7067.
(99) Bussi, G.; Donadio, D.; Parrinello, M. *J. Chem. Phys.* **2007**, *126*, 014101.
(100) Ramage, R.; Green, J.; Muir, T.; Ogunjobi, O.; Love, S.; Shaw, K. *Biochem. J.* **1994**, *299*, 151−158.
(101) Gullingsrud, J.; Kosztin, D.; Schulten, K. *Biophys. J.* **2001**, *80*, 2074−2081.
(102) Colombo, G.; Marrink, S. J.; Mark, A. E. *Biophys. J.* **2003**, *84*, 2331−2337.
(103) Jeon, J.; Voth, G. A. *Biophys. J.* **2008**, *94*, 3497−3511.
(104) Yefimov, S.; van der Giessen, E.; Onck, P. R.; Marrink, S. J. *Biophys. J.* **2008**, *94*, 2994−3002.
(105) Louhivuori, M.; Risselada, H. J.; van der Giessen, E.; Marrink, S. J. *Proc. Natl. Acad. Sci. U.S.A.* **2010**, *107*, 19856−19860.
(106) Rui, H.; Kumar, R.; Im, W. *Biophys. J.* **2011**, *101*, 671−679.
(107) Ollila, O. H. S.; Louhivuori, M.; Marrink, S. J.; Vattulainen, I. *Biophys. J.* **2011**, *100*, 1651−1659.
(108) Steinbacher, S.; Bass, R.; Strop, P.; Rees, D. C. *Curr. Top. Membr.* **2007**, *58*, 1−24.
(109) Blount, P.; Sukharev, S. I.; Schroeder, M. J.; Nagle, S. K.; Kung, C. *Proc. Natl. Acad. Sci. U.S.A.* **1996**, *93*, 11652−11657.
(110) de Jong, D. H.; Singh, G.; Bennett, W. F. D.; Arnarez, C.; Wassenaar, T. A.; Schäfer, L. V.; Periole, X.; Tieleman, D. P.; Marrink, S. J. *J. Chem. Theory Comput.* **2013**, *9*, 687−697.
(111) van Dijk, M.; Wassenaar, T. A.; Bonvin, A. M. J. J. *J. Chem. Theory Comput.* **2012**, *8*, 3463−3472.
(112) Fennell, C. J.; Bizjak, A.; Vlachy, V.; Dill, K. A. *J. Phys. Chem. B* **2009**, *113*, 6782−6791.
(113) Masunov, A.; Lazaridis, T. *J. Am. Chem. Soc.* **2003**, *125*, 1722−1730.

(114) Schutz, C. N.; Warshel, A. *Proteins* **2001**, *44*, 400−417.
(115) Hummer, G.; Pratt, L. R.; Garcia, A. E. *J. Phys. Chem.* **1996**, *100*, 1206−1215.
(116) Figueirido, F.; Del Buono, G. S.; Levy, R. M. *J. Phys. Chem. B* **1997**, *101*, 5622−5623.
(117) Bogusz, S.; Cheatham, T. E.; Brooks, B. R. *J. Chem. Phys.* **1998**, *108*, 7070−7084.
(118) Peter, C.; van Gunsteren, W. F.; Hünenberger, P. H. *J. Chem. Phys.* **2003**, *119*, 12205.
(119) Villa, A.; Peter, C.; van der Vegt, N. F. A. *J. Chem. Theory Comput.* **2010**, *6*, 2434−2444.
(120) Radzicka, A.; Wolfenden, R. *Biochemistry* **1988**, *27*, 1664−1670.
(121) Baron, R.; Trzesniak, D.; de Vries, A. H.; Elsener, A.; Marrink, S. J.; van Gunsteren, W. F. *ChemPhysChem* **2007**, *8*, 452−461.
(122) Dolenc, J.; Missimer, J. H.; Steinmetz, M. O.; van Gunsteren, W. F. *J. Biomol. NMR* **2010**, *47*, 221−235.
(123) Schmid, N.; Eichenberger, A. P.; Choutko, A.; Riniker, S.; Winger, M.; Mark, A. E.; van Gunsteren, W. F. *Eur. Biophys. J.* **2011**, *40*, 843−856.
(124) Kabsch, W.; Sander, C. *Biopolymers* **1983**, *22*, 2577−2637.
(125) Riniker, S.; Eichenberger, A. P.; van Gunsteren, W. F. *J. Phys. Chem. B* **2012**, *116*, 8873−8879.
(126) Darré, L.; Tek, A.; Baaden, M.; Pantano, S. *J. Chem. Theory Comput.* **2012**, *8*, 3880−3894.
(127) Bekker, H.; van den Berg, J. P.; Wassenaar, T. A. *J. Comput. Chem.* **2004**, *25*, 1037−1046.

dx.doi.org/10.1021/jp311533p | *J. Phys. Chem. B* XXXX, XXX, XXX−XXX